Supporting Information

Effective Stabilization of Long Cycle Lithium−Sulfur Batteries Utilizing In−Situ Prepared Graphdiyne−Modulated Separators

Jing Wang, [†‡] Kun Wang, [†*] Ze Yang, [†] Xiaodong Li, [†] Juan Gao, [†] Jianjiang He, [†] Ning Wang, [§] Huanlei Wang, [‡] Yanliang Zhang, [&] Changshui Huang [†*]

[†]Qingdao Institute of Bioenergy and Bioprocess Technology, Chinese Academy of Sciences, 189 Songling Road, Qingdao266101, P. R. China

[‡]Ocean University of China, 238 Songling Road, Qingdao 266101, P. R. China

[§]Shandong University, 27 Shanda Nanlu, Jinan 250100, P.R. China.

[&]Thermo Fisher Scientific., Ltd, 27 Xin Jinqiao Road, Shanghai 201206, P. R. China

E−mail: huangcs@qibebt.ac.cn; wang_kun@qibebt.ac.cn.

Materials characterization

The morphology of GDY−modulated PP and bare PP separators was measured by field emission scanning electron microscopy (FESEM, HITACHI S−4800), respectively. The TEM image of exfoliated GDY after as−prepared GDY−modulated PP dissolved in hot methylbenzene to remove the PP base, and the precipitation GDY products were filtered and collected, then measured by transmission electron microscopy (TEM, H−7650) apparatus. The X−Ray photo electron spectrometer (XPS) was tested on VG Scientific ESCA Lab220i−XL X−Ray photo electron spectrometer, using Al Ka radiation as the excitation sources. The Raman spectra were recorded at room temperature using a Thermo Scientific DXRXI system with excitation from an Ar laser at 532 nm. The in−situ Raman measurement was operated through a Thermo Scientific™ DXR™xi, as diagrammatized in Figure S1. Raman imaging microscope and an in−situ optical electrochemical cell with sandwich configuration and quartz window, as shown in Figure S1. The Raman imaging microscope spectra were collected over a 100 μm × 100 μm area with different change state. Raman images were presented in which the image contrast was generated by the changes in the strength of the acetylene bond. The Galvanostatic charge/discharge results were obtained by a LAND−CT2001 instrument. Cyclic voltammetry (CV) and electrochemical impedance spectroscopy (EIS) results was carried out using a CHI760 electrochemical work station.

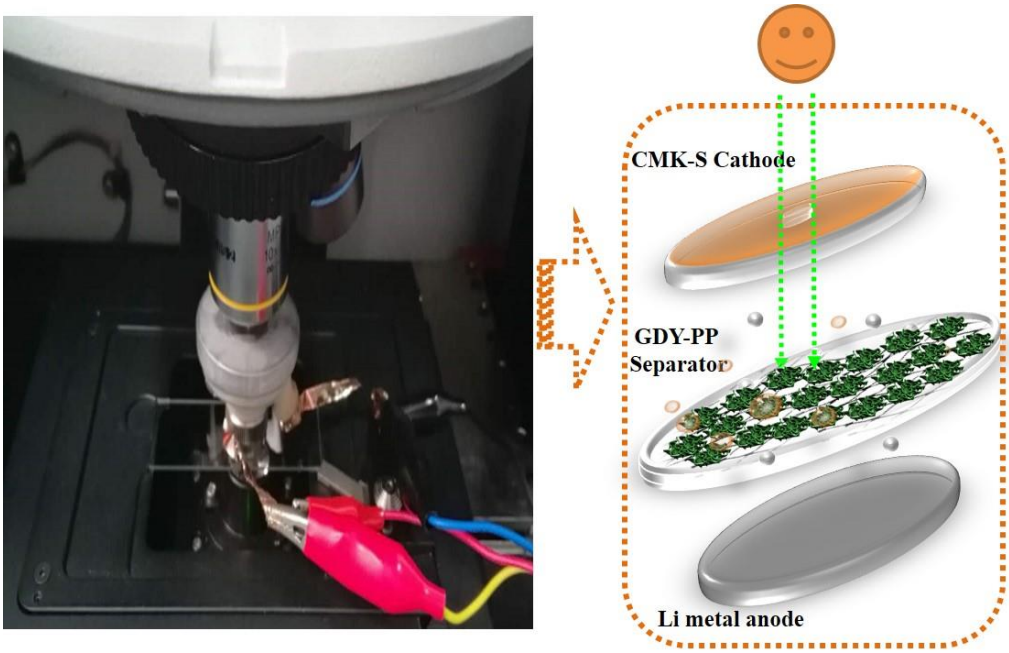

Figure S1. Experimental setup for the in situ example showing the electrochemical cell mounted on the stage of a Raman imaging microscope.

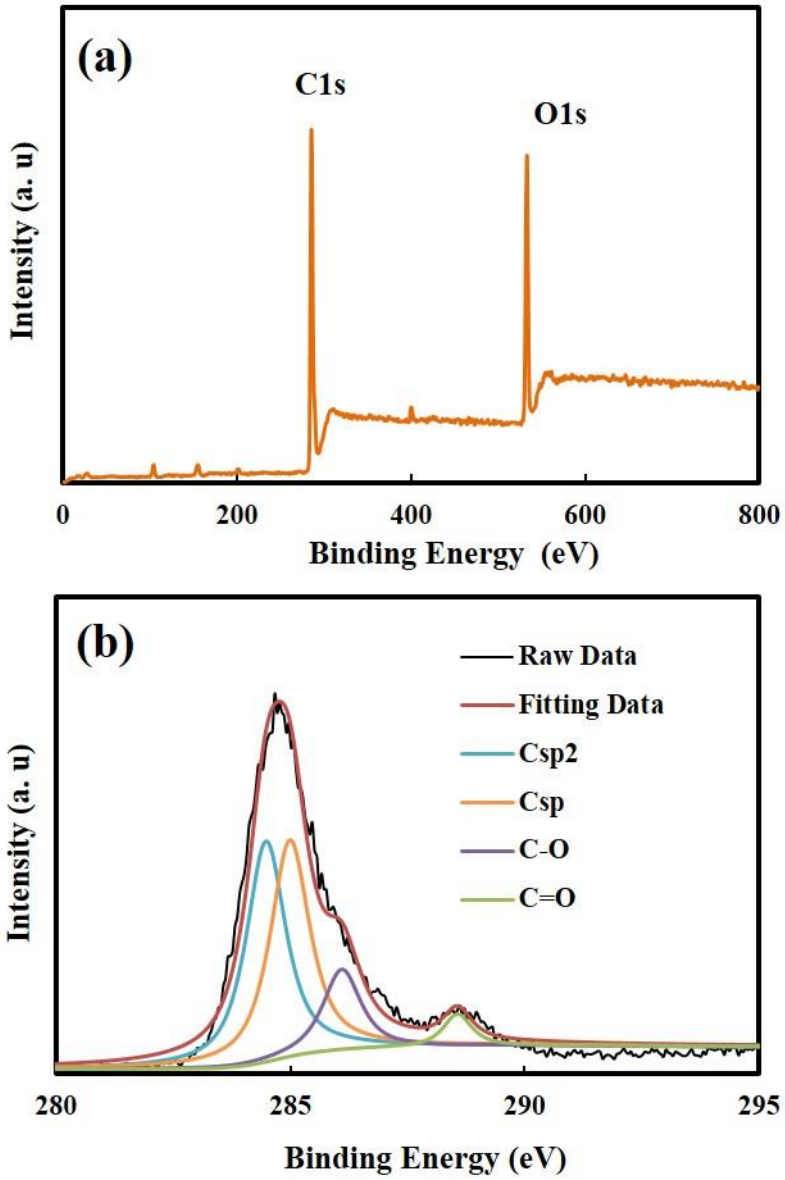

Figure S2. (a) The XPS survey of exfoliated GDY; (b) XPS survey of the chemical composition analysis for C1s (b) of exfoliated GDY.

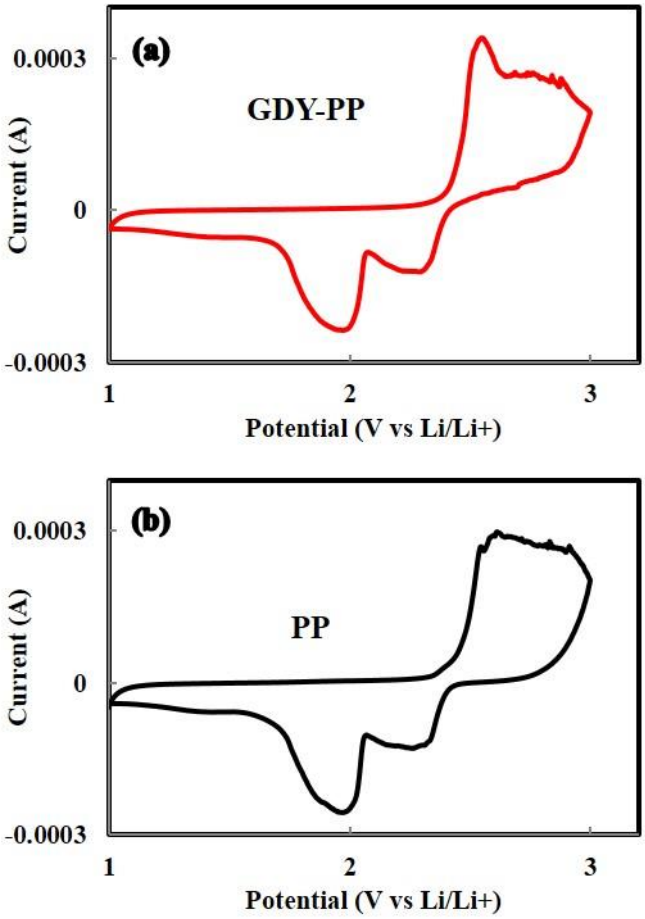

Figure S3. CV curves of the GDY–PP (a) and PP (b) based cells at first cycles with a scan rate of 0.1 mV s^{-1}.

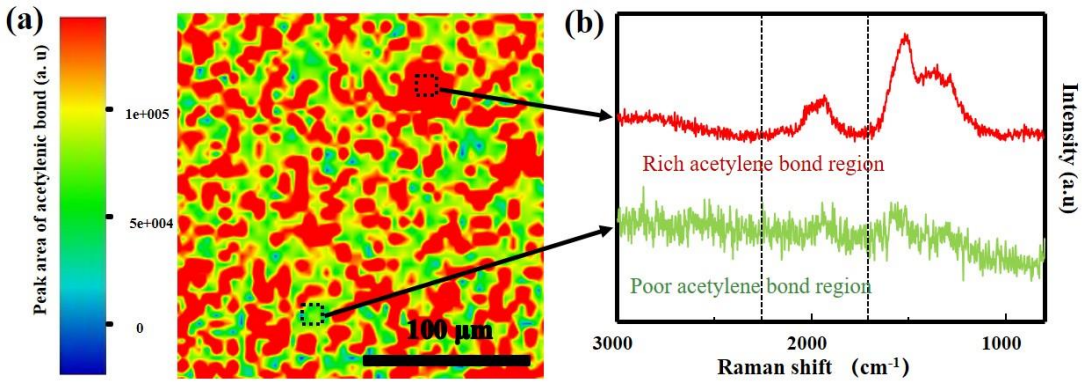

Figure S4. (a) In−situ Raman images of GDY−PP based separator from the area of acetylene peaks (specific peak region 1800~2200 cm^{-1}) at initial state; (b) The Raman spectrum corresponding to specific regions.

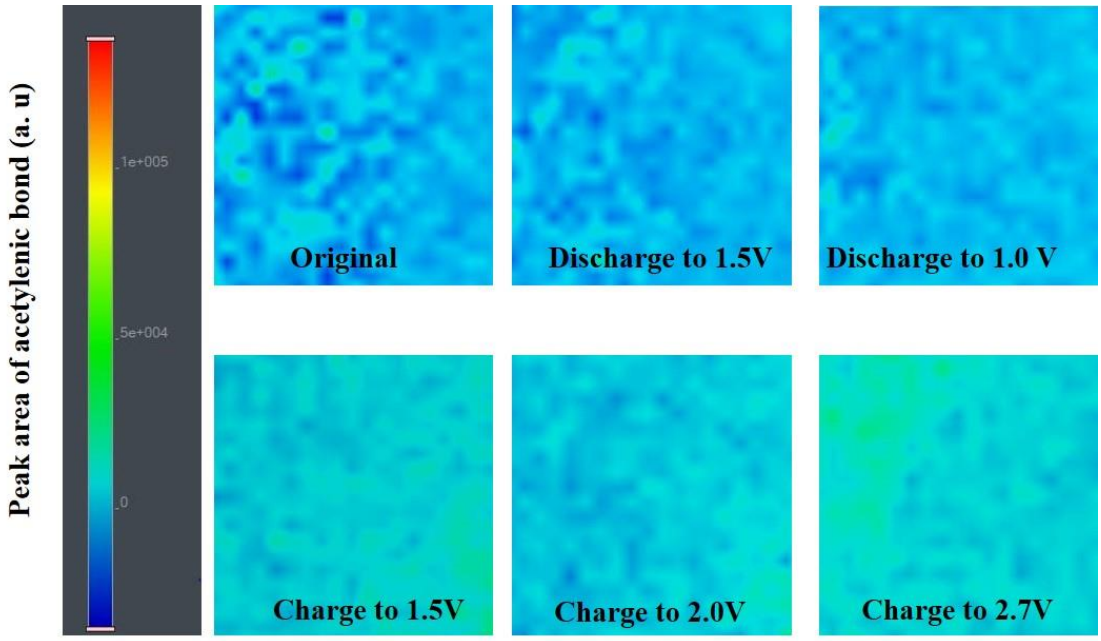

Figure S5. In−situ Raman images of PP based separator from the area of acetylene peaks (specific peak region 1800~2200 cm^{-1}) with different state of charge during the electrochemical process.

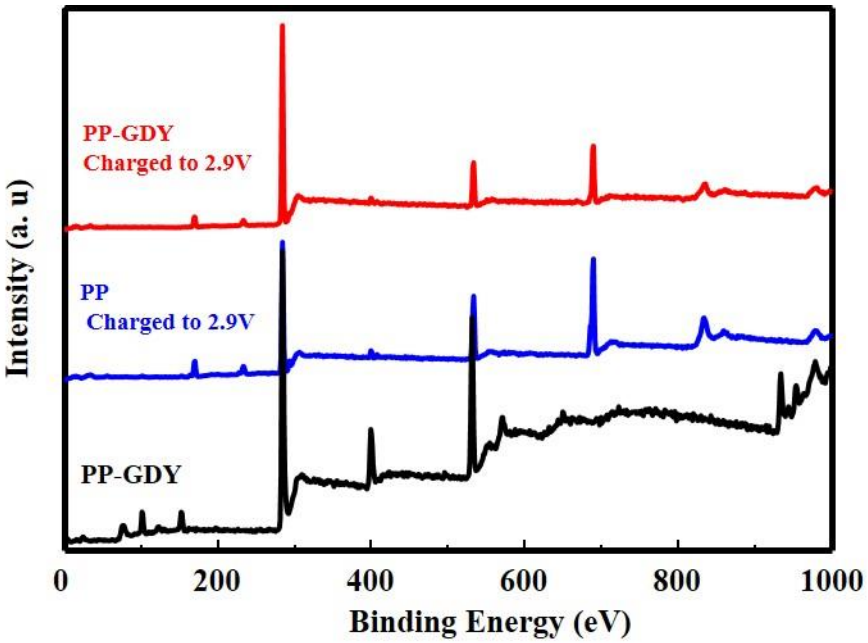

Figure S6. The XPS survey of GDY–PP, PP separator based cells after 300 cycles.

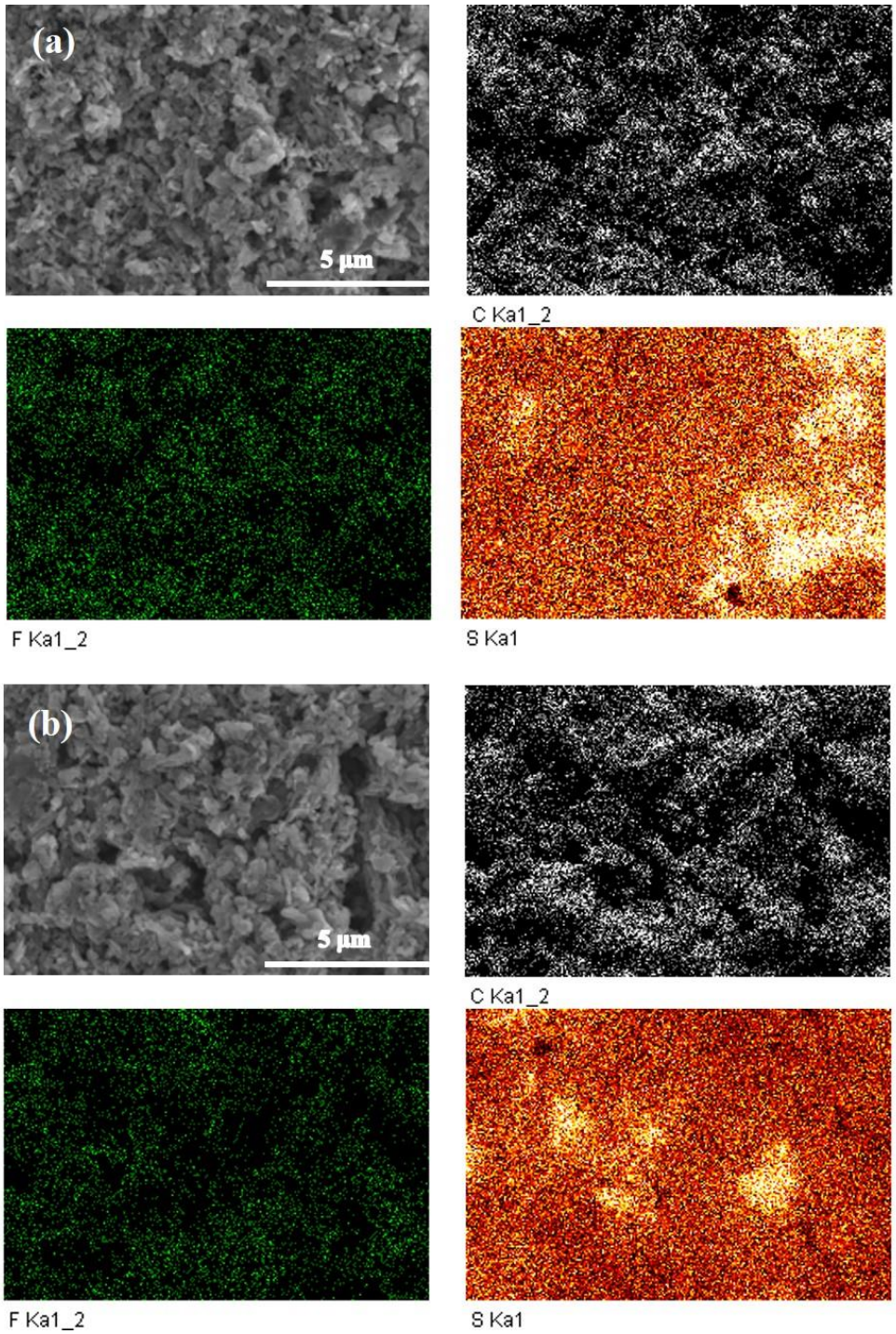

Figure S7. The EDX elemental mapping of Li anode from the PP (a) and GDY−PP (b) separators based cells charged to 2.7 V at 300 cycles.

Table S1. Comparison of Li−S batteries performance with previous reports involving carbon–coated composite separators using carbon/sulfur cathodes.

Materials	Sulfur content (wt %)	Current (C−rate)	Cycles	Initial discharge capacity (mAh g^{-1})	Capacity retention (mAh g^{-1})	Capacity decay per cycle	Years/ Refs
GDY	70	1	600	1396	412	0.095%	**This work**
CNT−zeolitic	80	0.2	100	1588.4	870.3	0.45%	2019[1]
Ketjen Black /TiO_2	67.5	0.5	100	996.7	804.3	0.192%	2019[2]
Graphene/CuS	53.3	0.2	200	1302	639	0.19%	2019[3]
MXene/ESM	67	0.5	250	1185	876	0.104%	2018[4]
rGO/MoS_2	70	0.2	500	1122	368	0.116%	2018[5]
CNFs@ZrO_2	70	0.2	500	1181	759	0.098%	2018[6]
C_3N_4	45	0.2	200	990	829	0.5%	2018[7]
CNFs/MnO_2	80	0.5	200	1156	856	0.191%	2017[8]
SWCNTs	80	0.2	300	953	501	0.18%	2016[9]
Mesoporous Carbon	60	0.2	500	1378	683	0.081%	2015[10]
PANi−MWCNT	60	0.2	100	1020	709	0.3%	2015[11]
MCNT/PEG	60	0.5	200	1283	727	0.12%	2015[12]
Carbon	60	0.2	200	1389	828	0.20%	2014[13]
PEG/Carbon	70	1	500	1300	780	0.1088%	2014[14]
Super P	60	0.5	500	1350	740	0.09%	2014[15]

References

1. Wu, F.; Zhao, S. Y.; Chen, L.; Lua, Y.; Su, Y. F.; Jia, Y. N.; Bao, L. Y.; Wang, J.; Chen, S.; Che, R. J. Metal–Organic Frameworks Composites Threaded on the CNT Knitted Separator for Suppressing the Shuttle Effect of Lithium Sulfur Batteries. *Energy Storage Materials.* **2018**, *14*, 383–391, DOI: 10.1016/j.ensm.2018.06.009.

2. Lin. S.; Cai Y. Y.; Yang. J.; Ruan. F. X.;Wu, J.; Sireesh, B.; Yao, X.; Gao. J .K.; Yao, J. M. Entrapment of Polysulfides by a Ketjen Black&Mesoporous TiO_2 Modified Glass Fiber Separator for High Performance Lithium–Sulfur Batteries. *J. Alloys and Compounds.* **2019**, *779*, 412–419, DOI: 10.1016/j.jallcom.2018.11.261.

3. Lia, H.; Suna, L.; Zhao, Y.; Tan, T.; Zhang, Y. A novel CuS/Graphene–Coated Separator for Suppressing the Shuttle Effect of Lithium/Sulfur Batteries. *Appl. Surf. Sci.* **2019**, 466, 309–319, DOI: 10.1016/j.apsusc.2018.10.046.

4. Yin, L. X., Xu, G. Y.; Nie, P.; Dou, H.; Zhang, X. G. MXene Debris Modified Eggshell Membrane as Separator for High–Performance Lithium–Sulfur Batteries. *Chem. Eng. J.* **2018**, 352, 695–703, DOI: 10.1016/j.cej.2018.07.063.

5. Tan, L.; Li, X.; Wang, Z.; Guo, H.; Wang, J. Light Weight Reduced Graphene Oxide@ MoS2 Interlayer as Polysulfide Barrier for High–Performance Lithium–Sulfur Batteries. *ACS Appl. Mater. Interfaces* **2018**, *10*, 3707–3713, DOI: 10.1021/acsami.7b18645.

6. Lia, Y.; Zhu, J.; Shi, R.; Dirican, M.; Zhu, P.; Yan, C.; Jia, H.; Zang, J.; He, J.; Zhang, X. Ultrafine and Polar ZrO_2–inlaid Porous Nitrogen–Doped Carbon Nanofiber as Efficient Polysulfide Absorbent for High–Performance Lithium–Sulfur Batteries with Long Life Span. *Chem. Eng. J.* **2018**, *349*, 376–387, DOI: 10.1016/j.cej.2018.05.074.

7. Huangfu, Y.; Zheng, T. T.; Zhang, K.; She, X. J.; Xu, H.; Fang, Z.; Xie, K. Y. Facile Fabrication of Permselective g–C3N4 Separator for Improved Lithium–Sulfur Batteries. *Electrochimica Acta*, **2018**, *272*, 60–67, DOI: 10.1016/j.electacta.2018.03.149.

8. Lai, Y.; Wang, P.; Qin, F.; Xu, M.; Li, J.; Zhang, K. A Carbon Nanofiber@Mesoporous δ–MnO_2 Nanosheet–Coated Separator for

High–Performance Lithium–Sulfur Batteries. *Energy Storage Mater*. **2017**, *9*, 179–187, DOI: 10.1016/j.ensm.2017.07.009.

9. Chang, C.–H.; Chung, S.–H. Manthiram, A. Effective Stabilization of a High–Loading Sulfur Cathode and a Lithium–Metal Anode in Li–S Batteries Utilizing SWCNT–Modulated Separators. *Small* **2016**, *12*, 174–179, DOI: 10.1002/smll.201502505.

10. Balach, J.; Jaumann, T.; Klose, M.; Oswald, S.; Eckert, J.; Giebeler, L. Functional Mesoporous Carbon–Coated Separator for Long–Life, High–Energy Lithium–Sulfur Batteries. *Adv. Funct. Mater.* **2015**, *25*, 5285–5306, DOI:10.1002/adfm.201502251.

11. Chang, C.–H.; Chung, S.–H.; Manthiram, A. Ultra–Light Weight PANiNF/MWCNT–Functionalized Separators with Synergistic Suppression of Polysulfide Migration for Li–S Batteries with Pure Sulfur Cathodes. *J. Mater. Chem. A* **2015**, *3*, 18829–18834, DOI:10.1039/C5TA05053G.

12. Wang, G.; Lai, Y.; Zhang, Z.; Li, J.; Zhang, Z. Enhanced Rate Capability and Cycle Stability of Lithium–Sulfur Batteries with a Bifunctional MCNT@PEG–Modified Separator. *J. Mater. Chem. A* **2015**, *3*, 7139–7144, DOI: 10.1039/c4ta07133f.

13. Chung, S.-H.; Manthiram, A. Bifunctional. Separator with a Light–Weight Carbon-Coating for Dynamically and Statically Stable Lithium-Sulfur Batteries. *Adv. Funct. Mater.* **2014**, *24*, 5299, DOI: 10.1002/adfm.201400845.

14. Chung, S.–H.; Manthiram, A. A Polyethylene Glycol–Supported Microporous Carbon Coating as a Polysulfi de Trap for Utilizing Pure Sulfur Cathodes in Lithium–Sulfur Batteries. *Adv. Mater*. **2014**, *26*, 7352–7357, 10.1002/adma.201402893.

15. Yao, H.; Yan, K.; Li, W.; Zheng, G.; Kong, D.; Seh, Z.; Narasimhan, V.; Liang, Z.; Cui, Y. Improved Lithium–Sulfur Batteries with a Conductive Coating on the Separator to Prevent the Accumulation of Inactive S–Related Species at the Cathode–Separator Interface. *Energy Environ. Sci.* **2014**, *7*, 3381–3390, DOI: 10.1039/C4EE01377H.